J. Fluid Mech. (1994), *vol.* 269, *pp.* 283–299

Supercooling in hypersonic nitrogen wind tunnels

By WAYLAND C. GRIFFITH,[1] WILLIAM J. YANTA[2] AND WILLIAM C. RAGSDALE[2]

[1] Mars Mission Research Center, North Carolina State University, Raleigh, NC 27695-7921, USA

[2] Aerodynamics Branch, Naval Surface Warfare Center–White Oak, Silver Spring, MD 20903-5000, USA

(Received 22 July 1992 and in revised form 14 January 1994)

Recent experimental observation of supercooling in large hypersonic wind tunnels using pure nitrogen identified a broad range of non-equilibrium metastable vapour states of the flow in the test cell. To investigate this phenomenon a number of real-gas effects are analysed and compared with predictions made using the ideal-gas equation of state and equilibrium thermodynamics. The observed limit on the extent of supercooling is found to be at 60% of the temperature difference from the sublimation line to Gibbs' absolute limit on phase stability. The mass fraction then condensing is calculated to be 12–14%. Included in the study are virial effects, quantization of rotational and vibrational energy, and the possible role of vibrational relaxation and freezing in supercooling. Results suggest that use of the supercooled region to enlarge the Mach–Reynolds number test envelope may be practical. Data from model tests in supercooled flows support this possibility.

1. Introduction

The purpose of this paper is to investigate the behaviour of supercooled nitrogen in wind tunnels of Mach number $M = 10$ and above at high unit Reynolds numbers. Recent experiments on supercooling (metastable states of the vapour phase below the saturation and sublimation lines) by Hudson *et al.* (1989) showed that the free-stream flow consistently supercools by 20–25 K before condensation appears in the Mach 10, 14 and 18 nitrogen tunnels at the Naval Surface Warfare Center (NSWC), White Oak, MD. To explore the gasdynamics of such flows in these and other tunnels a number of real gas processes not significant to standard wind tunnel operations must be considered. Of practical interest is the possibility that the range of Mach and Reynolds number accessible for aerodynamic testing may be enlarged.

Oswatitsch (1956) first recognized supercooling as a non-equilibrium gasdynamic process in supersonic wind tunnels using moist air as the working fluid. He observed a delay in the formation of condensation nuclei after the fluid had cooled below the saturation line for water followed by a zone of very rapid particle growth, a 'condensation shock', leading to an equilibrium mixture of vapour and water droplets. Methods used to avoid this problem included drying and preheating the air supply. For all subsequent tunnel designs conventional wisdom has been to select the test-cell state to lie near or outside the saturation region. Daum & Gyarmathy (1968) compiled data on the onset of condensation in a large variety of hypersonic wind tunnels operating at that time and noted fairly consistent patterns for nitrogen and for air, but little further attention was given the subject during the next 20 years.

High-performance high-pressure hypersonic tunnels require very high supply temperatures where intermolecular forces and vibrational energy excitation produce

significant departures from a calorically perfect ideal gas. If expansion in a tunnel nozzle is too rapid then vibrational relaxation effects may lead to non-equilibrium and freezing of some of the vibrational energy. The NSWC tunnel nozzles were designed to be very long for this reason, recognizing that the increased fluid transit time might reduce the exent of supercooling.

Culotta & Richards (1970) showed that nitrogen expanding in hypersonic wind tunnels will behave as a perfect gas (ideal-gas equation of state with constant specific heats) beyond the point where the Mach number reaches a value of 9, meaning that the downstream flow can be analysed using the familiar aerodynamic relations for constant specific heat ratio. This is common practice in the testing community. For deep supercooling the vapour temperature may approach 10 K so the effects of rotational energy quantization and intermolecular virial effects need to be evaluated.

The paper is organized in the following way. First, general thermodynamic relations and criteria for phase stability are reviewed. Then the available experimental data on the properties of equilibrium nitrogen needed for this work are presented. Vibrational and rotational energy are discussed in §4. Introduction of real gas properties into the steady compressible flow equations in §5 provides a basis for identifying where various real-gas and non-equilibrium effects must be considered. Section 6 gives the experimental data on supercooling and discusses measurement methods. Section 7 presents results of aerodynamic model testing with supercooling. Lastly, an assessment of real-gas effects in the supercooled region and location of the spinodal are presented.

2. Thermodynamic relations and phase stability

The general thermodynamic relations needed for this analysis are those for a one-component vapour phase system with constant particle number. The first and second laws define internal energy u and entropy s in terms of the state variables p, $v = 1/\rho$, and T. Enthalpy h and Gibbs function g per unit mass are respectively given by

$$h = u + pv \quad \text{and} \quad g = h - Ts. \tag{1}$$

The specific heats at constant pressure and volume and the speed of sound are defined as

$$C_p = \left(\frac{\partial h}{\partial T}\right)_p, \quad C_v = \left(\frac{\partial u}{\partial T}\right)_v, \quad a^2 = \left(\frac{\partial p}{\partial \rho}\right)_s. \tag{2}$$

For real gases the internal energy is made up of temperature-dependent terms accounting for particle translational states and internal energy states, plus terms depending on both temperature and density arising from intermolecular forces,

$$u = \tfrac{3}{2}RT + E_{int} + \left(1 - T\frac{\partial}{\partial T}\right)\int_0^\rho \frac{(p - \rho RT)}{\rho^2}\,\mathrm{d}\rho. \tag{3}$$

The entropy can be calculated from

$$\mathrm{d}s = C_v\frac{\mathrm{d}T}{T} + \left(\frac{\partial p}{\partial T}\right)_v \mathrm{d}v. \tag{4}$$

The condition for thermodynamic equilibrium between the vapour and condensed phases, called by Gibbs (1961) the 'binodal' in the (p, v)-plane, is

$$g_{(1)} = g_{(2)}, \quad \text{and} = g_{(3)} \text{ for triple points.} \tag{5}$$

Here 1, 2, and 3 refer to vapour and condensed phases. This condition leads to the well-known Clausius–Clapeyron equations for the vaporization and sublimation lines in the (p, T)-plane.

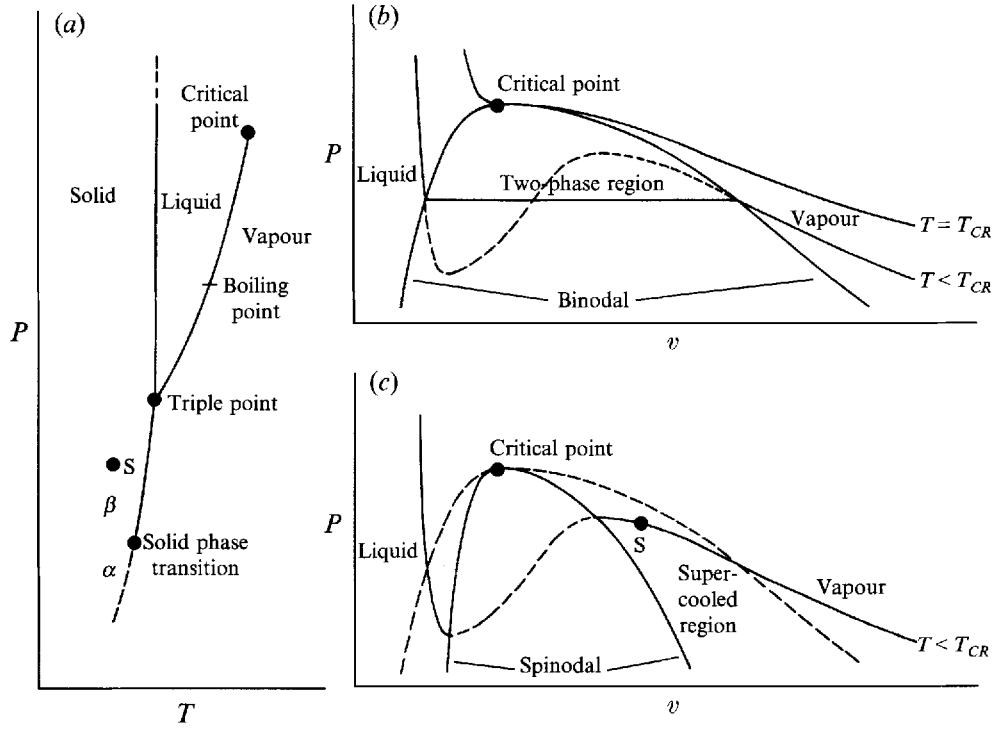

FIGURE 1. (*a*) Phase diagram in the (p, T)-plane showing the critical point, boiling point, triple point and the vaporization, sublimation and melting curves. The symbol S represents a typical metastable supercooled vapour state. (*b*) Sketch of (p, v)-plane with Van der Waals' equation for two values of T and Gibbs' binodal for thermodynamic phase equilibrium. (*c*) Similar to (*b*) but with Gibbs' spinodal as a stability limit for metastable states of supercooled gas and superheated liquid. Again S represents a supercooled state.

An absolute limit on phase stability is given by Gibbs as

$$\Delta T \Delta s - \Delta p \, \Delta v > 0. \tag{6}$$

It follows that the boundary of phase stability, called the 'spinodal' by Gibbs, is given by

$$\left(\frac{\partial p}{\partial v}\right)_T = 0 \quad \text{or} \quad \left(\frac{\partial T}{\partial s}\right)_p = 0. \tag{7}$$

Finally, the critical point is identified by condition (7) and

$$\left(\frac{\partial^2 p}{\partial v^2}\right)_T = 0 \quad \text{or} \quad \left(\frac{\partial^2 T}{\partial s^2}\right)_p = 0. \tag{8}$$

Simultaneous measurements of p, v and T have been made for nitrogen vapour over a wide range of states from very high p and T down to the vapour–liquid–solid triple point and the equilibrium phase boundaries determined experimentally. Naturally no direct experimental data are available for the non-equilibrium supercooled states between the binodal and spinodal lines. Extrapolation of real-gas properties into this region is needed.

General practice in smoothing state property data has been to expand the ideal-gas equation of state in a truncated power series whose form is chosen to reflect the nature

of the molecular force fields that determine the kinematics of intermolecular collisions. Numerous models are available. Here we will follow Gibbs in using Van der Waals' equation

$$(p+a/v^2)(v-b) = RT, \tag{9}$$

with a and b assumed to be constant, in order to gain a qualitative picture of the binodal and spinodal. From (7) the spinodal is given by

$$p_{sp} = 2a(v_{sp}-b)/v_{sp}^3 - a/v_{sp}^2, \quad RT_{sp} = 2a(v_{sp}-b)^2/v_{sp}^3. \tag{10}$$

The critical point is at the apex of both the binodal and spinodal. With the additional condition of (8)

$$v_c = 3b, \quad p_c = a/27b^2, \quad RT_c = 8a/27b. \tag{11}$$

Figures 1(a) and 1(b) shows sketches of the equilibrium phase boundaries in the (p, T)- and (p, v)-planes; figure 1(c) shows how the binodal is replaced by the spinodal as the phase boundary for metastable non-equilibrium supercooling and superheating. Point S shown in figures 1(a) and 1(c) represents a supercooled vapour state reached during isentropic expansion of the wind tunnel working gas.

For quantitative work use of the virial equation of state, an expansion in inverse powers of v, will be used;

$$pv/RT = 1 + B/v + C/v^2 + \ldots. \tag{12}$$

In principle the virial coefficients can be calculated from the intermolecular force fields of colliding molecules. In practice these quantum mechanical force fields can be obtained from basic particle dynamics only for the simplest elements: helium and hydrogen. For non-polar, nearly spherical species of greater molecular weight such as nitrogen the Leonard–Jones 6-12 model has been found to be particularly satisfactory. This will be discussed in the next section.

3. Property data for nitrogen

Vapour-phase properties of nitrogen between the triple point and 10000 atm and 1944 K have been compiled by the National Bureau of Standards (NBS) in TN 648 (1973) and a 32-coefficient expression for the equation of state given in virial form (see the Appendix). At the triple point, 0.1237 atm and 63.17 K, densities of the three phases in lbm/cu.ft are: vapour 0.0421, liquid 54.18, solid 59.01. Din (1961) gives expressions for the sublimation line from the triple point to the solid phase transition at 35.5 K and below. For most nitrogen wind tunnels of $M = 10$ and above isentropic expansion brings the gas to a state near sublimation.

The Leonard–Jones model for the potential energy field of colliding molecules has an inverse sixth-power attractive field and an inverse twelfth-power repulsive field with two parameters to be determined for the species colliding. Evaluation of the collision integrals for the viscosity, Joule–Thomson, and virial coefficients is discussed in Rossini (1955). The results for nitrogen based on data for viscosity and for the second virial coefficient are gratifyingly consistent are shown in table 1.

The use of these parameters in evaluating the collision integrals for the virial coefficient B in a gas with a Maxwellian velocity distribution function down to 28.5 K is given in Hirschfelder, Curtiss & Bird (1954). Computations for the third virial coefficient C have also been attempted but with conflicting results from different workers. This stems partly from the far more complex integrations involved and partly from the smaller and less certain database for C.

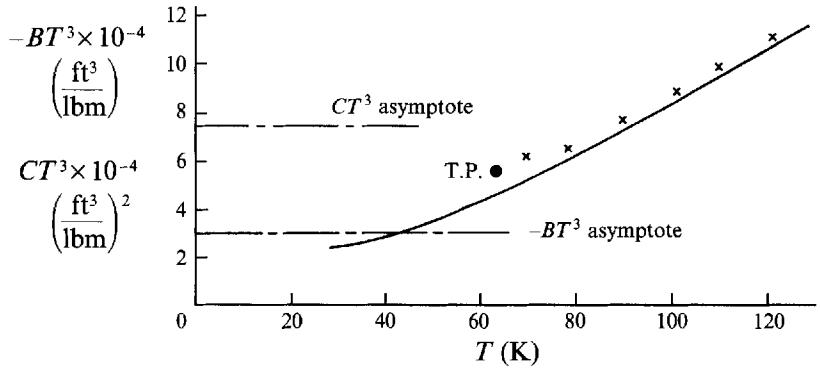

FIGURE 2. Virial coefficients B and C for (12). Shown are experimental values for B given by Din (1961) (×); as derived from triple-point data (●); values calculated using the Leonard–Jones model (——); and the low-temperature asymptotes according to the equation of state in NBS TN 648 (– ——– ——).

	Viscosity	Virial B
ϵ/k (K)	91.46	95.05
r_o (A)	3.681	3.698

TABLE 1. Leonard–Jones parameters determined from data

A comparison of values for the second virial coefficient B at very low temperatures is given in figure 2. Shown are some experimental data, the Leonard–Jones results just discussed, and the low-temperature asymptotes for B and C calculated using the equation of state from NBS TN 648 in the Appendix. In view of the consistency of these different sources and lacking any other basis on which to proceed we use the coefficients in Appendix A for B and C for estimating state properties and the spinodal in the supercooled region.

4. Internal energy states of the nitrogen molecule

Between about 20 K and 500 K nitrogen is accurately described as a calorically perfect gas with $C_v = 5R/2$. At lower temperatures the effects of energy quantization of rotational states (characteristic temperature $T_r = 2.847$ K) appear and at higher temperatures molecular vibration (characteristic temperature $T_v = 3390$ K) contributes to the internal energy.

The contribution of rotational energy states to specific heat reflects the quantum mechanical selection rules for nuclear spin and rotational quantum numbers. Using the expressions given by Gopal (1966) and Mayer & Mayer (1940) for nitrogen-14, calculations show that the effect on γ is less than 2% down to 5 K. Rotational relaxation times correspond to only a few collisions and can also be neglected in this study.

The nitrogen molecule is tightly bound, with the highest vibration frequency and longest vibrational relaxation time of any diatomic species. Experiments confirm the applicability of the mechanical resonance theory of Landau & Teller (1936) in which the vibrational energy of a gas changes according to a simple relaxation process for small vibrational quantum numbers. The vibrational relaxation time, τ, is a function

of pressure and temperature for each interacting species. Important to a later discussion is the observation that collisions between a molecule and a particulate or an unlike molecule may be more effective by many orders of magnitude from that for like-molecule collisions. The relaxation time for pure nitrogen is given by Vincenti & Kruger (1965) as

$$p\tau = 7.12 \times 10^{-3} \exp(1.91 \times 10^6 / T^{\frac{1}{3}}), \tag{13}$$

where the units are atm, μs and K. This is still the expression of choice for pure nitrogen (Anderson 1989). Resolution of a long-standing disparity of a factor of 5 to 70 between rates measured from shock waves and from expanding flows has recently been given by Sharma *et al.* (1992) who found that the disparity in rates between expansion and compression in spectroscopically clean nitrogen was within the ratio of 1:1.5.

5. Steady compressible flow of real gases

The thermodynamics of real gases have been used with the conservation equations for compressible flow to analyse hypersonic tunnel performance in a variety of ways. For analysing the free core flow in an existing tunnel, common practice is to assume quasi-steady isentropic flow with constant total enthalpy. With these assumptions the flow along streamlines is determined using

$$\mathrm{d}(\rho V A) = 0 \quad \text{(Mass)}, \tag{14}$$

$$-\mathrm{d}p + \rho V \,\mathrm{d}V = 0 \quad \text{(Momentum)}, \tag{15}$$

$$h_0 = u + pv + \tfrac{1}{2}\rho V^2 \quad \text{(Energy)}, \tag{16}$$

along with a real-gas equation of state and thermal property data.

Culotta & Richards (1970) introduced the concept of an equivalent perfect-gas flow, i.e. one having the same entropy and total enthalpy as the real flow. The two would become identical once the gas had expanded to a density and temperature where virial and vibrational energy effects became negligible. This was found to occur for tunnel expansion to $M = 9$ and above for the hypersonic tunnels at NSWC.

For the same total enthalpy and entropy at the tunnel supply state the equivalent perfect gas will always have a higher temperature T_{o1} than the real-gas value T_o. For pressure the equivalent perfect-gas value may be either higher or lower depending on the level selected. Figure 3 illustrates the situation for nitrogen. The locus of states for which P_o and the equivalent perfect-gas supply pressure P_{o1} are equal is shown as line 1. The standard operating points for some tunnels are shown. At pressures above about 100 atm the temperature corrections for internal energy are seen to be strongly enhanced by the effects of the (virial) force fields.

A Pitot tube in the test section will experience a pressure that is scarcely affected by virial factors since the fluid is in the range of ideal-gas behaviour. A stagnation temperature probe will read a total temperature that is not equal to either T_o or T_{o1} because total enthalpy rather than total temperature is the conserved property. Hollis, Griffith & Yanta (1991) gives the real-gas correction. Effects of vibrational energy lag in the stagnation flow onto a Pitot tube may be kept negligible by using a sufficiently large-diameter head.

If the tunnel design leads to a too rapid expansion cooling of the working gas, then vibrational energy lag may occur and a relaxation equation must be added to the set for solution. The problem of vibrational energy lag and freezing in wind tunnels has been studied extensively by Stollery & Park (1964) and others so that a qualitative

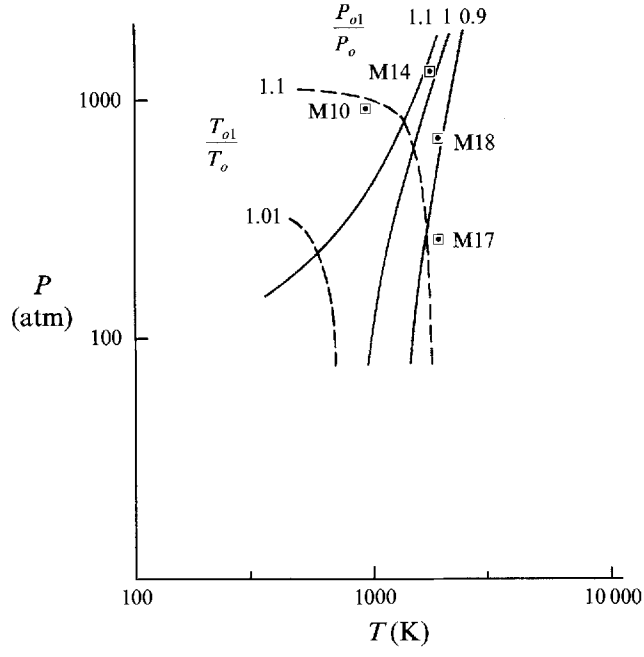

FIGURE 3. Plot of tunnel supply conditions showing contours of the ratios of perfect-gas pressure P_{o1} and temperature T_{o1} to real gas values P_o and T_o for the same entropy and enthalpy. Tunnel design points: M10, NSWC Tunnel 9 Mach 10 leg; M14, Mach 14 leg; M18, NSWC Tunnel 8A Mach 18; M17, NASA Langley Mach 17 continuous tunnel. A new mach 18 experimental nozzle throat for NSWC Tunnel 9 uses the Mach 14 supply system.

physical picture has appeared. Experimental detection of the extent of freezing is extremely difficult. Optical methods have been developed to measure vibrational-state populations but only those that do not require seeding the gas would be useful because a foreign species might well shorten the relaxation time. Theoretical analysis is complex because virial effects probably persist throughout the regions of non-equilibrium flow and freezing so a real-gas equation of state should be used in computations. For pure nitrogen some computations suggest that freezing may occur in the vicinity of the nozzle throat when the temperature has dropped to about 1000 K.

Without firm quantitative data for guidance, Tunnel 9 nozzles at NSWC were prudently designed to be very long (40 ft) to reduce the gas cooling rate. During calibration and subsequent use the staff conducted a thorough study of the free core flow and flow about a variety of model shapes to detect any evidence of some residual vibrational energy. The results were null. Three explanations may account for this; tunnel length is indeed sufficient to assure equilibration, trace contaminant species or particulates shorten the effective relaxation time, or lag occurs but late enough in the flow for the residual vibrational energy to be of no practical importance.

6. Supercooling and condensation

Oswatitsch (1956) was the first to investigate the quantitatively the non-equilibrium cooling of water vapour below its saturation temperature in supersonic wind tunnels. He observed a region of what we now call supercooling followed by the very rapid appearance and growth of particles leading to an equilibrium mixed flow of air and fine water droplets. These condensation shocks, as he called them, could under certain

State	P(mmHg)	T(K)	Mach	V(ft s^{-1})
Supercooled	0.049	16.7	13.5	3680
Condensed	0.116	41.5	9.38	3690

TABLE 2

circumstances couple with tunnel starting flow to choke the tunnel and prevent the formation of supersonic flow. Supercooling occurs because the process of particle nucleation is inhibited by a surface energy (or surface tension) barrier associated with the formation of very small particles from the vapour phase. Fluctuations of sufficient magnitude arise only infrequently to form an aggregation of critical size, i.e. a particle of that critical size where one more added molecule will cause it to grow and one less molecule will cause it to disappear again. The critical size predicted by theory for the condensible gases is typically a few hundred molecules.

A great deal of research has been done on nucleation and particle growth owing to its importance in this and other fields: cloud chambers, steam turbines, chemical plants and atmospheric physics. Wegener (1969), Blythe & Shih (1976), Gorbunov (1988) and others have clarified the processes of homogeneous and heterogeneous nucleation and developed theories for condensation in the condensible gases. Daum & Gyarmathy (1968) attempted to adapt the time-dependent nucleation model from condensible gases to their nitrogen wind tunnel data but did not obtain satisfactory results.

Subsequently it was realized that vapour supercooling and liquid superheating are somewhat complementary effects involving non-equilibrium metastable phase states limited by Gibbs' concept of the spinodal. Skripov (1974) studied metastable liquids in great detail and Shepherd & Sturtevant (1974) investigated the applicability of the concept to the explosion of Mt St. Helena. Their experimental data and that given by Gorbunov showed a perfectly smooth locus of states passing across the equilibrium phase-change line and a subsequent transition to mixed-phase equilibrium.

Previous experimental data on the transition between supercooling and equilibrium mixed-phase flow used photography to observe light scattering or absorption by the condensed particle cloud, static pressure taps to detect the local pressure rise resulting from the onset of condensation or simply the appearance of rapid signal variations which were interpreted as tunnel flow disturbances caused by condensation. There are no observation ports in the NSWC contoured nozzles so Hudson *et al.* (1989) developed two methods applicable to the straight cylindrical test cell which is 12 ft long and 5 ft in diameter. There the tunnel wall boundary layer is the order of 1 ft thick.

An analytical model was developed for the pressure read by a Pitot tube in a partially condensed flow and applied to data from a large number of tunnel run records. Films and video tapes showed marked darkening of the field at very early and very late run times when the supply temperature was low, clear evidence of condensation. During runs at standard conditions the supply temperature reached values sufficiently high that the test cell state entered the equilibrium vapour-phase region where no condensed particles could be expected. Since the data traces from the fixed Pitot monitors were in most cases the only source of information about the time history of the core flow, a computer program was written to iterate on the transition point. Once the transition was located, all the flow properties of the equilibrium partially condensed state and those of the associated supercooled pure vapour state were calculated.

Some data from a representative example are given in table 2 for transition occurring when the supply state was 301 psia, 624 K and the Pitot pressure was 0.220 psia. The

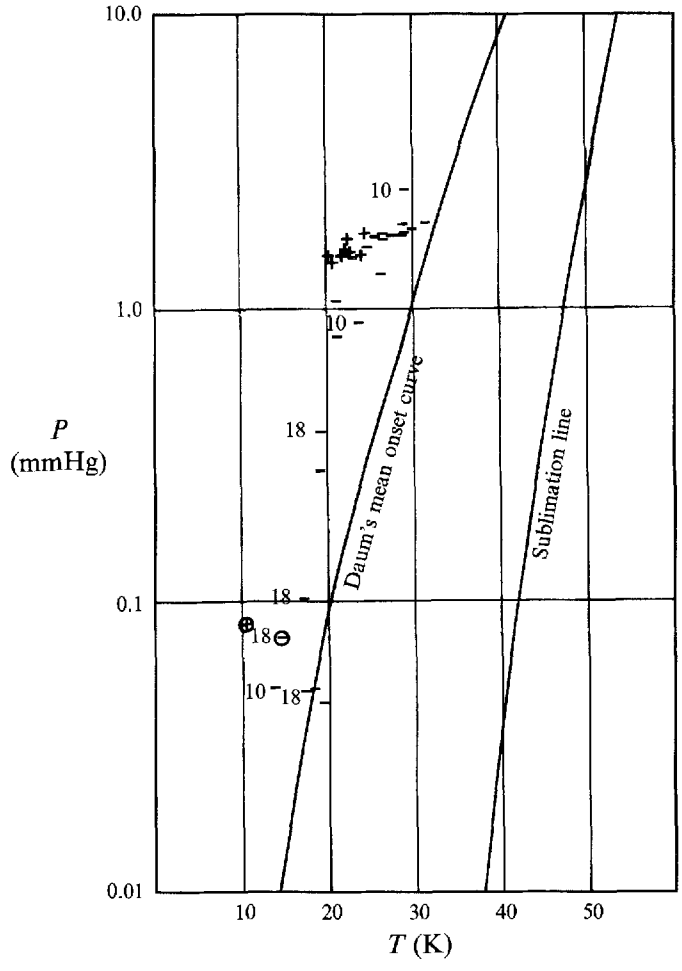

FIGURE 4. Log P *vs.* T plot for hypersonic nitrogen tunnel test section states. Shown are the sublimation line, Daums & Gyarmathy's (1968) mean experimental curve for onset of condensation, and Hudson *et al.*'s (1989) data from the NSWC tunnels. Symbols: −, disappearance of condensation at early run times; +, reappearance of condensation at late times. Data were not recorded long enough on all runs to pick up the return of condensed flow. Most data are for Mach 14; points marked (10) and (18) are for the Mach 10 and 18 nozzles. Two circled values are from Jones (1992) using the new experimental Mach 18 nozzle.

mass fraction condensed was 12.3%. The expanding flow crossed the sublimation line at 49 K, 2.11 mmHg. Instead of identifying a supercooled state in relation to the point where the isentropic flow crossed the sublimation line a more common practice is to give the isobaric supercooling ΔT. This is defined as temperature difference in degrees K between the supercooled state and a point on the sublimation line at the same pressure. For the case above $\Delta T = 23.4$ K. These results were later supported by data from the second new measuring device, a laser-light-scattering–photomultiplier detector which resolved the appearance and disappearance of condensed particles with better time resolution.

Figure 4 shows supercooling data in relation to the sublimation line for nitrogen. Included are Daum & Gyarmathy's mean onset curve, data from the fixed Pitot monitors taken during test runs and from Pitot rakes, and results from series of dedicated runs for which tunnel conditions were set to produce sucessively larger

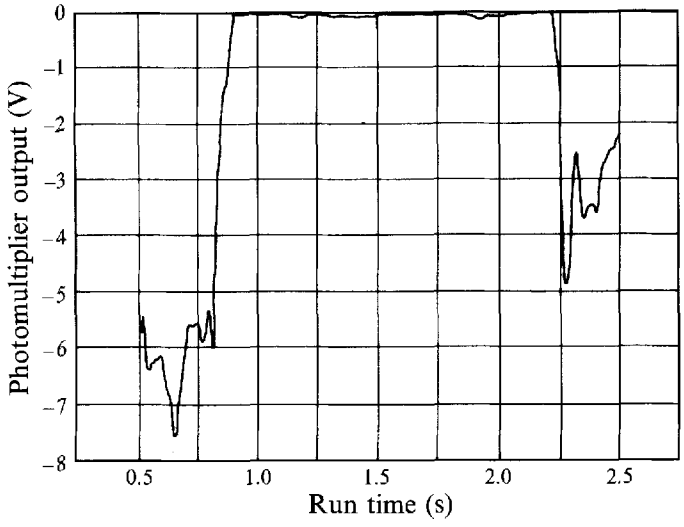

FIGURE 5. Time trace of photomultiplier voltage for a supercooled run in the Mach-14 tunnel indicating existence of condensation at early and late run times. From $t = 0.87$ to 2.24 s no scattered light was detected. This interval is in agreement with the period of supercooled flow identified from Pitot data.

amounts of supercooling until condensed flow persisted throughout the entire run. The data give a fairly consistent pattern; transition occurs at 20–30 K isobaric supercooling with the critical mass fraction condensed calculated as being 12–14 %. The heat release to the fluid and the removal of molecules from the gas phase by this rather large mass fraction distinguishes nitrogen condensation in hypersonic tunnels from the processes previously observed in supersonic flows. It also accounts in part for the sensitivity of Pitot pressure to condensation.

Data from the Pitot rake show very poor flow quality at early run times when a large amount of condensation is present, as would be expected while the tunnel is operating far from the design condition. Upon the disappearance of condensation the rake data exhibit uniform readings in the core suggesting a flow quality comparable to that seen at standard operating conditions. This will be discussed further in §7 on model testing.

The laser–photomultiplier system consisted of a 20 mW linearly polarized Helium–Neon laser at 632.8 nm, a collecting lens, and a photomultiplier detector. The unfocused laser beam was transverse to the tunnel axis and it was estimated that the backscattered light was detected from a volume 1.0 mm in diameter and 25 mm long. The optical collecting system for the photomultiplier had an f-number of 10; its axis was at an angle of 20° from that of the laser beam. The particles were expected to be too small to detect individually. The intensity of scattered light was found to be strongly dependent upon orientation of the collection optics with respect to the polarization vector. Scattering theory indicates that this would be the case if the particles were less than 0.1 μm.

Figure 5 shows the (negative) photomultipler voltage output for a supercooled run in the Mach-14 tunnel. The signal is zero from 0.87 s to 2.26 s, indicating the absence of detectable light scattering. This interval is in agreement with the period of supercooled flow identified from the Pitot data. The rapid monotonic changes over about 0.2 s immediately before and after this period can be accounted for by changes in the mass fraction of nitrogen condensed, and hence quantity of particles, during early warmup and late cooldown. As mentioned previously, the mass fraction at

transition to supercooled states is 12–14%. The large oscillations in signal at the earliest and latest times correspond to similar fluctuations in Pitot pressure and are interpreted as starting transients.

Nucleation and particle growth models exhibit a dwell period after which the number of nuclei of critical size for further growth increase rapidly, followed by increasingly fast addition to particle mass until thermodynamic equilibrium between the two phases is achieved. The fluid transit time available, from the point where flow crosses the sublimation line to the test cell, is 6–8 ms (2 ms in the smaller Mach-18 tunnel). The response frequency of the photomultiplier data system is 60 KHz, probably fast enough to resolve the structure of the particle growth region were it not masked by the strong variations in tunnel conditions just as transition to or from supercooling occurs.

Mention was made previously of the design decision to make the Tunnel 9 nozzles very long as a means for reducing vibrational energy lag and freezing, while realizing that the increased flow time might lead to early condensation. This is in fact not the case; data from these tunnels are close to Daum's mean onset curve. Another aspect worth consideration is a direct interaction between vibrational relaxation and nucleation. Energy frozen in molecular vibrational states during nozzle expansion could influence particle nuclation and growth. The quantum of vibrational energy is approximately a hundred times the mean molecular kinetic energy at condensation and would almost certainly be released upon encounter with a nucleating particle, thus prolonging the mean time for particles of critical size to form. Molecular internal energy has been included in theoretical models for condensation of the condensible gases. For nitrogen wind tunnels there is still insufficient experimental evidence to decide whether or not this effect is significant.

Dust and other particulates in the tunnel core flow could provide heterogeneous nucleation as an alternative path to homogeneous nucleation in the formation of nitrogen condensate. Tunnel starting processes are likely to create some particulates that will be most prevalent in the initial transient flow and tunnel wall boundary layers. No quantitative data on particle size and number distribution in the quasi-steady core flow are available. For future work with supercooling and theoretical modelling of condensation, instrumentation to measure these quantities is desirable.

7. Wind tunnel testing in supercooled hypersonic flow

The practical application of supercooling in hypersonic nitrogen flow as described here is to expand the range of operating conditions in wind tunnels. Substantial increases in Reynolds number as well as moderate increases in Mach number were observed during the investigations of supercooling in the NSWC tunnels. Using a modified nozzle the Mach-14 facility has been operated at Mach 18 with supercooled test cell flow, and with flow quality comparable to that obtained in normal tunnel operation at Mach 14. In order for model testing to be feasible, however, not only the tunnel flow but also the flow around the model must be of good quality. The possibility of condensation in the model flow must be considered.

The feasibility of testing in supercooled wind tunnel flow must ultimately be based on actual test experience and in fact a reasonably comprehensive base of experience can be cited. During the initial calibration of the Mach 10 configuration, and also in the smaller Mach-18 research tunnel, it was noted that good-quality wind tunnel flow could be obtained at a level of supercooling $\Delta T = 8$ K. Standard production testing has been performed in both these facilities at this level of supercooling for many years,

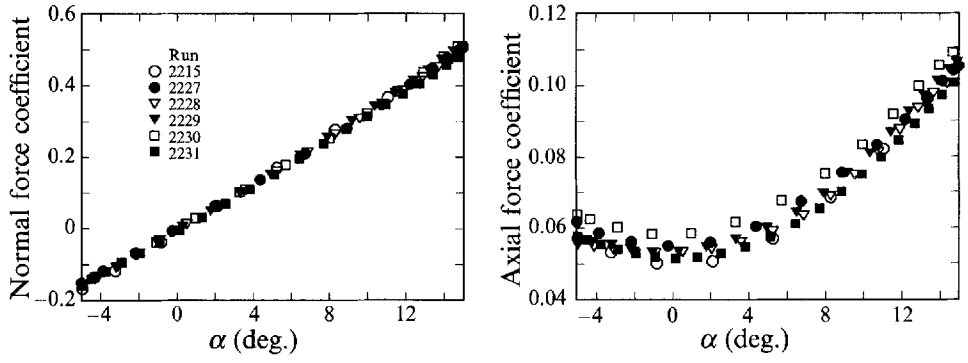

FIGURE 6. Normal force and axial force coefficients *vs.* angle of attack for a 7° half-angle cone model in the Mach-14 tunnel. Run conditions are for constant Reynolds number from the standard condition with no supercooling to the limit of supercooling.

Run	P_0(atm)	T_0(K)	M	Re ft^{-1} ($\times 10^6$)	P(mmHg)	T(K)	ΔT(K)
			Sharp cone				
2215	1409	1839	14.3	3.65	2.4	52	0
2229	633	1149	14.5	3.44	0.98	30	17
2228	619	1092	14.5	4.08	1.03	28	19
2227	352	768	14.7	4.05	0.52	18	27
2230	324	676	14.7	4.50	0.52	16	29
2231	789		flow partially condensed				(31)
			Blunt cone				
2232	1394	1816	14.4	3.59	2.2	50	0
2235	846	1455	14.3	3.41	1.5	40	8
2234	275	735	14.5	3.37	0.41	18	27

TABLE 3. Test conditions for cone models at Mach 14

with satisfactory results. Test measurements in the Mach-10 facility have included local surface pressures and heating rates as well as aerodynamic forces. Experience with the Mach-18 tunnel has been limited to force measurements.

More recently, tests have been run in the Mach-14 facility with sharp and blunt cone models to explore the feasibility of testing at Mach 14 with the larger levels of supercooling comparable to those reported here. Measurements have included surface pressures and heating rates along with aerodynamic forces over a range of angles of attack. Table 3 gives the test conditions for some of these runs. Each set begins with the standard supply condition shown in figure 3 (no supercooling), followed by runs with increasing amounts of supercooling until condensation in the tunnel flow was observed. Supply conditions were chosen to keep both Mach and Reynolds numbers the same to isolate effects of supercooling.

Figures 6 and 7 plot the normal and axial force coefficients as functions of angle of attack for the sharp cone and blunt cone, respectively. The models had a 7° half-angle with a base diameter of 14.4 in. The blunt cone had a hemispherical nose with bluntness ratio of 22.31%.

Portions of the supercooled flow around models which pass through shock waves of sufficient strength or are included in the boundary layer will experience heating and as a result condensation is unlikely to occur even upon re-expansion. Condensation will

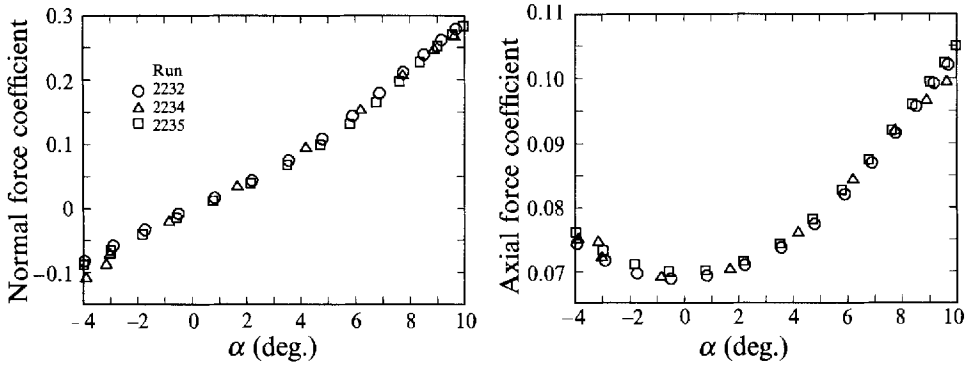

FIGURE 7. Similar to figure 6 but for the blunt cone.

be most likely to occur within portions of the flow on the leeward side of a model at angle of attack. Model base pressures are usually the lowest encountered in testing, and are not more than a factor of 5 lower than the tunnel static pressure. The possibility of condensation in a model flow field due to the expansion of an already supercooled flow to pressures less than the tunnel static was addressed in Mach 14 experimental tests with a flat plate model by Lederer *et al.* (1990).

The possibility of condensation in portions of model flow can never be ruled out completely, and its occurrence would certainly invalidate any flow field survey and local surface measurements in the vicinity. Nevertheless, the experience cited above indicates that a reasonably broad range of practical testing is possible in supercooled hypersonic flow. This is particularly true for the measurement of aerodynamic fores since the fact that they are integrated quantities makes them relatively insensitive to localized effects.

8. Virial effects in the supercooled region and the spinodal as a limit

The density of nitrogen vapour at the triple point differs by less than 1 % from the value calculated using the perfect-gas equation. As long as tunnels were designed with operating points outside the sublimation line, real-gas effects were negligible. Isentropic expansion deep into the supercooled region results in states of higher density. Using (4) and the virial equation of state given in the Appendix, (A 1), the relation for an isentropic change from some state 1 to state 2 is given by

$$\frac{\Delta S}{R} = 0 = \tfrac{3}{2}\ln\frac{T_2}{T_1} - \ln\frac{\rho_2}{\rho_1} - \int_1^2 \left[\rho\left(2\frac{\mathrm{d}B}{\mathrm{d}T} + T\frac{\mathrm{d}^2B}{\mathrm{d}T^2}\right) + \frac{\rho^2}{2}\left(2\frac{\mathrm{d}C}{\mathrm{d}T} + T\frac{\mathrm{d}^2T}{\mathrm{d}T^2}\right)\right]\mathrm{d}T$$
$$- \int_1^2 \left[\left(B + T\frac{\mathrm{d}B}{\mathrm{d}T}\right)\mathrm{d}\rho + \rho\left(C + T\frac{\mathrm{d}C}{\mathrm{d}T}\right)\mathrm{d}\rho\right]. \quad (17)$$

The two leading terms are just those for a perfect gas. Two sets of calculations illustrate the magnitude of the virial corrections to perfect-gas predictions for states deep in the supercooled region. In both we will compare isentropic flows from states where the expanding tunnel flow passes through $T = 300$ K and reaches the test cell at 20 K. Values of the entropy are chosen to arrive at test cell pressures of 1.0 mmHg and 0.10 mmHg, which may be seen from figure 4 as lying near the observed limits of supercooling.

First compare real-gas and perfect-gas flows starting from 300 K and 17.20 atm,

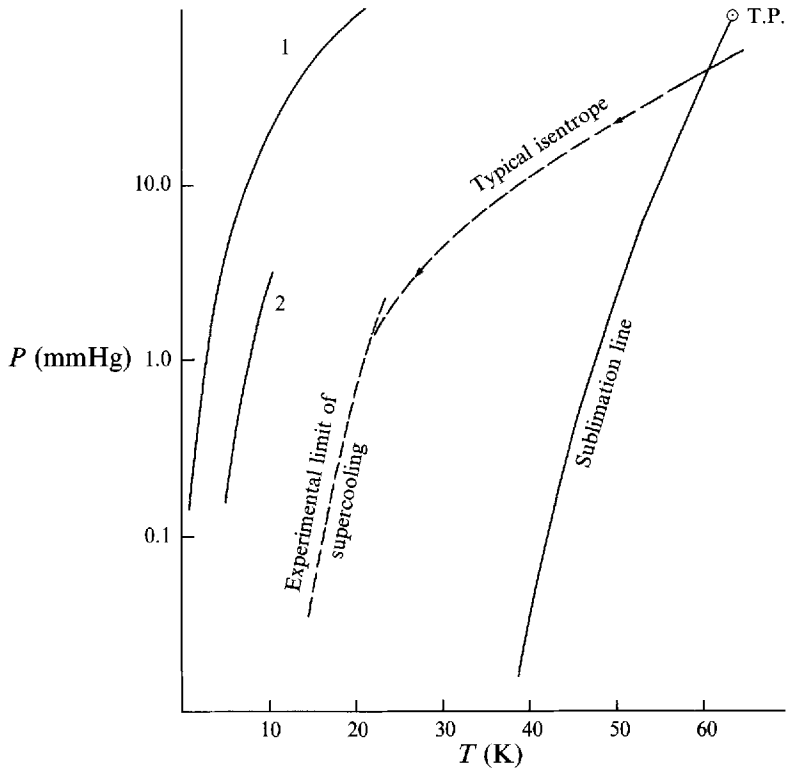

FIGURE 8. Spinodal calculated with constant Van der Waal coefficients fitted to triple point data (curve 1); using variable coefficients based on the virial equation of state (curve 2); the experimental limit of supercooling; and the sublimation line.

with both expanding to 20 K. The resulting states are: for real gas $T = 20$ K, $p = 1.0000$ mmHg; and for perfect gas $T = 20$ K and $p = 1.0341$ mmHg. The real-gas state is lower in pressure and density by 3.4% than that calculated in the customary way using perfect gas theory. This difference reflects cummulative changes from integration along an isentropic path and as such is larger than the departure of the real-gas state from the perfect-gas state at 20 K and 1.0 mmHg where the virial terms for $p/\rho RT$ are 1, 0.0022, and 0.000018, respectively.

The second example calculated is similar except that the starting point is 300 K and 1.72 atm. The difference between real- and perfect-gas values is 0.37%, probably not detectable by conventional measurement methods.

The spinodal, defined by (7), is an absolute thermodynamic limit to supercooling. As the state of a fluid approaches the spinodal, fluctuations in density increase in frequency and amplitude and eventually form a sufficient number of nuclei of critical size for condensation to occur. Location of the spinodal for nitrogen in the range of pressures and temperatures of interest according to figure 4 may be estimated using constant values for the Van der Waals coefficients a and b from triple-point data as the lowest temperature and pressure for which direct experimental values are available. This results in curve 1 shown in figure 8. As an absolute stability limit, this line has the required qualitative property of lying to the left of the Daum & Gyarmathy and NSWC supercooling limits but does not have quantitative value.

When the low-temperature asymptotes for virials B and C based on the NBS equation of state (see the Appendix) are used, an improved location for the spinodal

may be obtained. The result is shown as curve 2 in figure 8, which indicates that the observed limit of supercooling lies at 60% of the temperature difference between the sublimation line and the spinodal. The consistent pattern of the experimental data suggests that for nitrogen at very low temperatures the onset of condensation is being influenced by approach to the spinodal, where molecular theory would indicate that fluctuations provide the physical mechanism for thermodynamic phase change. That the limit of supercooling is being determined by a criterion based on thermodynamic state is a possibility that must be evaluated by developments in nucleation and growth models using nitrogen properties at the prevailing conditions.

9. Discussion and conclusions

Measurement methods used to study supercooled flows in hypersonic wind tunnels using pure nitrogen are described and the role of real-gas effects investigated. These include non-equilibrium, quantization and relaxation of rotational and vibrational internal energy states, and intermolecular forces.

A fairly consistent limit of 20–30 K isobaric supercooling over two orders of magnitude in pressure was observed, located at 60% of the temperature difference from the sublimation line to Gibbs's absolute limit on phase stability. The mass fraction then condensing is calculated to be 12–14%. Data from supercooled flows at Mach, 10, 14 and 18 taken in the NSWC tunnels indicated uniform test cell core flow of quality comparable to that obtained under standard tunnel operating conditions. With condensation present the tunnel flow was very non-uniform, as expected when running far from the design condition.

Exploratory tests with a number of standard models run at varying levels of supercooling showed negligible difference from data taken at standard operating conditions. If tunnel operation in the supercooled region proved practical for aerodynamic model testing, then appreciable gains in Reynolds number and modest gains in Mach number might be made. For this, not only the tunnel flow but also the model flow would have to be of good quality, i.e. free of condensation. Actual feasibility of testing in supercooled flow must be based on test experience with the complex models of future design interest.

Common practice in reducing wind tunnel test data for Mach numbers above 9 has been to use perfect-gas relations, well justified outside the sublimation line. Evaluation of the accuracy of this approximation to real-gas effects appearing in the supercooled shows variances of only a few percent, probably not enough to justify a change in current data reduction routines using a constant value of $\gamma = 1.4$ throughout the supercooled region.

The possibility that some residual vibrational energy is frozen into the flow has long been of concern, but its presence has not been verified from flow measurements. Since particle nucleation and growth might be strongly affected by release of this internal energy, further theoretical developments on the limits of supercooling would be of interest.

This work was done under a cooperative agreement between North Carolina State University, Raleigh and The Naval Surface Warfare Center, White Oak with support from the USN-USAF-NASA Hypersonics Research Program, Contract NAGW-1072 and the Mars Mission Research Center, NASA Contract NAGW-1331.

Appendix

The equation of state for nitrogen in National Bureau of Standards TN 648 covers the range from the triple point to 3500 R and 1.818 to 150000 psia in virial form with 32 parameters For this work we use just the first three terms

$$p/\rho RT = 1+\rho B+\rho^2 C, \tag{A 1}$$

with the second and third coefficients given as

$$B = (N_1 T+N_2 T^{\frac{1}{2}}+N_3+N_4/T+N_5/T^2)/RT \tag{A 2}$$

and

$$C = (N_6 T+N_7+N_8/T+N_9/T^2)/RT, \tag{A 3}$$

where

$$N_1 = 0.00136, \quad N_6 = 0.000105,$$
$$N_2 = 0.107, \quad N_7 = -0.0013,$$
$$N_3 = -0.244, \quad N_8 = 0.000143,$$
$$N_4 = 34.10, \quad N_9 = 18470.$$
$$N_5 = -4224.$$

From the energy and entropy relations, (3) and (4),

$$C_v = \tfrac{5}{2}R-2RT\rho\frac{\mathrm{d}B}{\mathrm{d}T}-RT^2\rho\frac{\mathrm{d}^2B}{\mathrm{d}T^2}-\left(2RT\frac{\mathrm{d}C}{\mathrm{d}T}+RT^2\frac{\mathrm{d}^2C}{\mathrm{d}T^2}\right)\frac{\rho^2}{2} \tag{A 4}$$

and

$$\left(\frac{\partial p}{\partial T}\right)_\rho = R\rho+R\left(B+\frac{\mathrm{d}B}{\mathrm{d}T}\right)\rho^2+R\left(C+T\frac{\mathrm{d}C}{\mathrm{d}T}\right)\rho^3. \tag{A 5}$$

At the lowest temperatures and pressures of interest in supercooling the two factors N_5 and N_9 with their inverse cube of the temperature dominate and were used in locating the asymptotes for B and C in figure 2 and for estimating the position of the spinodal (curve 2 in figure 8) from (7).

REFERENCES

ANDERSON, J. D. 1989 *Hypersonic and High Temperature Gas Dynamics*. McGraw Hill.

BLYTHE, P. & SHIH, C. J. 1976 Condensation shocks in nozzle flows. *J. Fluid Mech.* **76**, 593–621.

CULLOTA, S. & RICHARDS, B. E. 1970 Method for determining conditions in real nitrogen expanding flows. *VKI TN* 58.

DAUM, F. L. & GYARMATHY, G. 1968 Condensation in hypersonic wind tunnels. *AIAA J.* **6**, 458.

DIN, F. 1961 *Thermodynamic Functions of Gases*, Vol. 3. Butterworths.

GIBBS, J. W. 1961 *The Scientific Papers*, Vol. 1. Dover.

GOPAL, E. R. S. 1966 *Specific Heats at Low Temperatures*. Plenum.

GORBUNOV, V. N. 1988 *Non-Equilibrium Condensation in High Speed Gas Flows*. (Translated from Russian.) Gordon & Breach.

HIRSCHFELDER, J. O., CURTISS, C. F. & BIRD, R. B. 1954 *Molecular Theory of Gases and Liquids*. Wiley.

HOLLIS, B., GRIFFITH, W. & YANTA, W. 1991 Analysis of a Fine-Wire Thermocouple Stagnation Temperature Probe for Use in Hypersonic Flows in Nitrogen. *IEEE Publication* 91 CH3028-8, 14th ICIASF.

HUDSON, S. T., GRIFFITH, W. C., LEDERER, M., RAGSDALE, W. C. & YANTA, W. J. 1989 Condensation shocks in hypersonic nitrogen tunnels. *AIP Conf. Proc. 208: Current Topics in Shock Waves; 17th Intl Symp. on Shock Waves & Shock Tubes* (ed. Y. W. Kim). pp. 784–9.

JONES, K. 1992 Boundary layer study on nozzle wall at hypersonic velocities, PhD thesis, N.C. State University, Raleigh.

LANDAU, L. & TELLER, E. 1936 Zur Theorie der Shalldispersion. *Phys. Z. Sowjetunion* **10**, 34.

LEDERER, M., YANTA, W., RAGSDALE, W., HUDSON, S. & GRIFFITH, W. 1990 Condensation in hypersonic nitrogen wind tunnels. *AIAA Paper* 90-1392.

MAYER, J. E. & MAYER, M. G. 1940 *Statistical Mechanics*. Wiley.

NATIONAL BUREAU OF STANDARDS TN 648 1973 *Thermophysical Properties of Nitrogen from the Fusion Line to 3500 R for Pressures to 150,000 psia*. US Dept. of Commerce.

OSWATITSCH, K. 1956 *Gas Dynamics*. Academic.

ROSSINI, F. D. (ED.) 1955 *Thermodynamics and Physics of Matter*, pp. 360–372. Princeton.

SHARMA, S. P., RUFFIN, S. M., GILLESPIE, W. D. & MEYER, S. A. 1992 Nonequilibrium vibrational population measurements in an expanding flow using spontaneous Raman spectroscopy. *AIAA Paper* 92-2855.

SHEPHERD, J. E. & STURTEVANT, B. 1974 Rapid evaporation at superheat limit. *J. Fluid Mech.* **121**, 379–402.

SKRIPOV, V. P. 1974 *Metastable Liquids*, p. 203. (Translated from Russian). Wiley.

STOLLERY, J. L. & PARK, C. 1964 Computer solutions to the problem of vibrational relaxation in hypersonic nozzle flows. *J. Fluid Mech.* **19**, 113–123.

VINCENTI, W. G. & KRUGER, C. H. 1965 *Introduction to Physical Gas Dynamics*. Wiley.

WEGENER, P. P. 1969 *Non-Equilibrium Flows*, Part I. Dekker.